ELSEVIER

Marine and Petroleum Geology 19 (2003) 1257–1274

Marine and Petroleum Geology

www.elsevier.com/locate/marpetgeo

Atypical heat-flow near gas hydrate irregularities and cold seeps in the Baikal Rift Zone

Maarten Vanneste[a,*], Jeffrey Poort[a], Marc De Batist[a], Jan Klerkx[b]

[a]*Renard Centre of Marine Geology, Ghent University, Ghent B-9000, Belgium*
[b]*International Bureau of Environmental Sciences, Brussels, Belgium*

Received 13 July 2002; received in revised form 30 January 2003; accepted 1 February 2003

Abstract

In this paper, we address the irregular behaviour and geometry of the gas hydrate stability zone (HSZ) inferred from reflection seismic data in relation to heat-flow measurements. The study area lies in the hanging wall of the *Posolsky* fault in the Southern Baikal Basin (SBB). Side-scan sonar imagery already revealed an undulating antithetic active fault structure and several isolated active vent structures. Remarkably, these fluid discharge structures occur only where the base of the hydrate stability zone (BHSZ), as inferred from seismic reflection profiles, is fluctuating and discontinuous, independent of lake floor morphology. The correlation between the interpreted BHSZ and heat-flow data across the *Malenki* seep is reasonable. On a seismic profile south of the fluid escape features, the BHSZ is expressed as an oscillatory, but continuous reflection, and shows poor correlation with heat-flow measurements. In nearly all cases, measured heat-flow exceeds inferred heat-flow. Additionally, the local inferred minima are anomalously low compared to the expected background values in the SBB. These observations suggest that the present-day hydrate accumulation and its (meta-)stability are more complicated than originally suspected. The limited area of these anomalies, their amplitudes and their occurrence in the immediate vicinity of faults and fluid escape features suggest that fluid convection cells disturb local gas hydrate stability conditions.

Keywords: Lake Baikal; Gas hydrates; heat-flow; Fluid flow; Base of hydrate stability zone; Bottom-simulating reflection; Gas migration

1. Introduction: gas hydrates in Lake Baikal

Lake Baikal is the world's only confined fresh water basin with both direct and indirect evidence of gas hydrates (Golmshtok, Duchkov, Hutchinson, & Khanukayev, 1997, 2000; Vanneste, De Batist, Golmshtok, Kremlev & Versteeg, 2001). Their occurrence (Fig. 1) was first suggested by the presence of bottom-simulating reflections (BSRs) on multi-channel seismic (MCS) data in 1989 (Hutchinson et al., 1991), but it was not before 1997 that more details about their distribution became available (Golmshtok et al., 1997), based on MCS data acquired in 1992. Clear indications for hydrate accumulations are found in the Southern (SBB) and Central Baikal Basins (CBB), in areas more or less symmetrical to the Selenga Delta (Fig. 1), the main source for the supply of terrigenous organic material to the lake basins. The continuous BSR cuts across the folded and faulted stratigraphic reflections and mimics the lake floor morphology. The thickness of the hydrate stability zone (HSZ), inferred from the sub-bottom depth of the BSR, ranges from 35 to 450 m (Golmshtok et al., 1997). In 1999, a Belgian–Russian expedition was devoted to a more detailed study of gas hydrates in the SBB, using medium to high-frequency acoustic sources (30–400 Hz). The results of the multi-frequency acoustic analyses of the hydrate-bearing sediments in Lake Baikal were recently discussed (Vanneste, 2000; Vanneste et al., 2001).

In the framework of the Baikal Drilling Project (BDP), gas hydrate samples were collected in a borehole, on 121 and 161 m sub-bottom depth in coarse sandy turbidites enriched in plant debris in the axial part of the SBB (1428 m water depth, position: N51°47.9′–E105°29.3′; Fig. 2) (Kuzmin et al., 2000b). No information from intermediate depths is available due to poor core recovery. The borehole did not penetrate the base of the hydrate stability zone (BHSZ). On the single-channel (SC) medium-resolution seismic profiles across the drill site, a weak BSR is observed

* Corresponding author. Present address: Department of Geology, University of Tromsø, N-9037 Tromø, Norway.
E-mail address: maarten.vanneste@ig.uit.no (M. Vanneste).

0264-8172/03/$ - see front matter © 2003 Elsevier Science Ltd. All rights reserved.
doi:10.1016/S0264-8172(03)00019-9

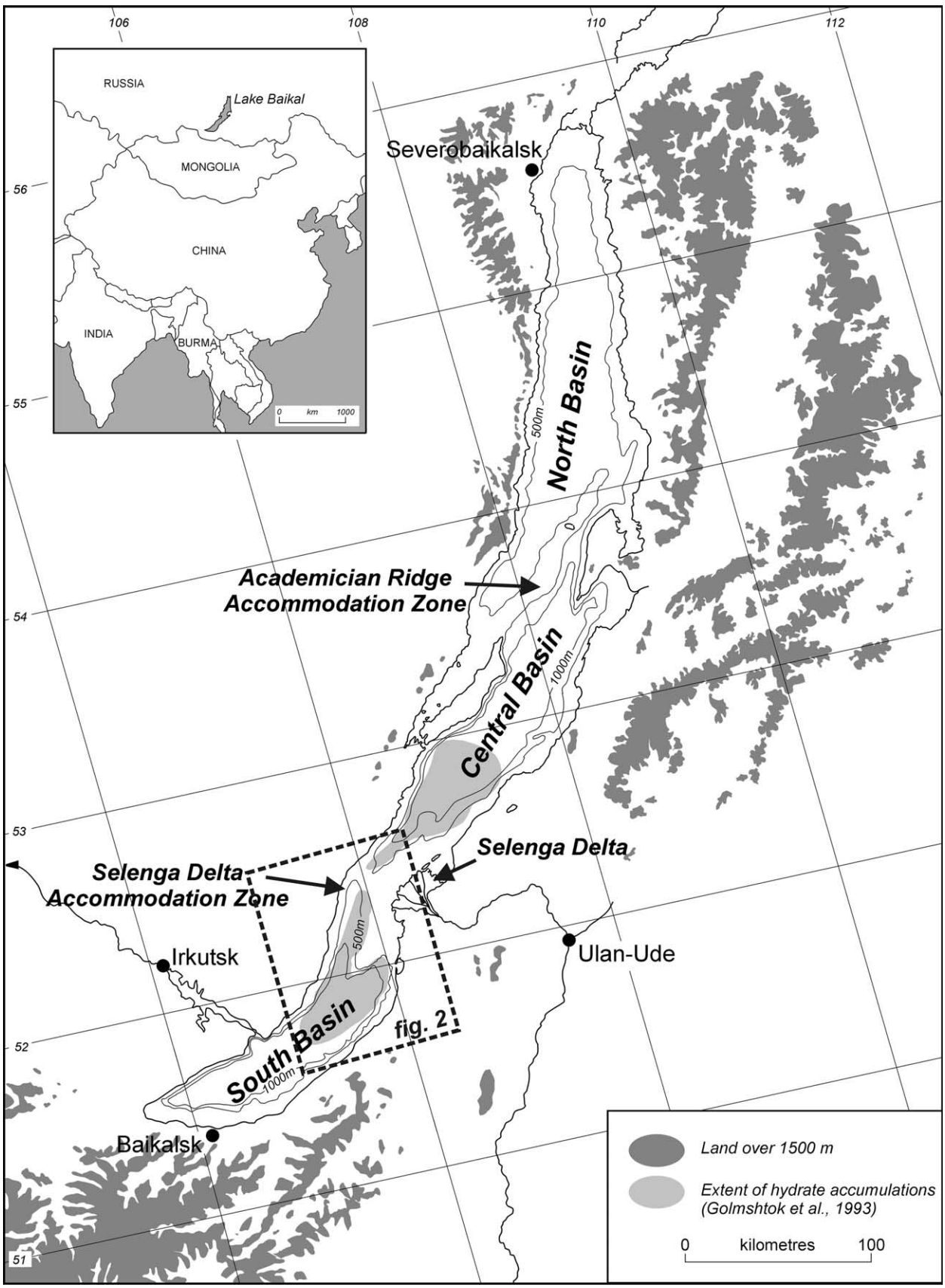

Fig. 1. Location map of Lake Baikal and its rift basins in Siberia (Vanneste et al., 2001). The dashed box indicates the study area. See Fig. 2 for more details.

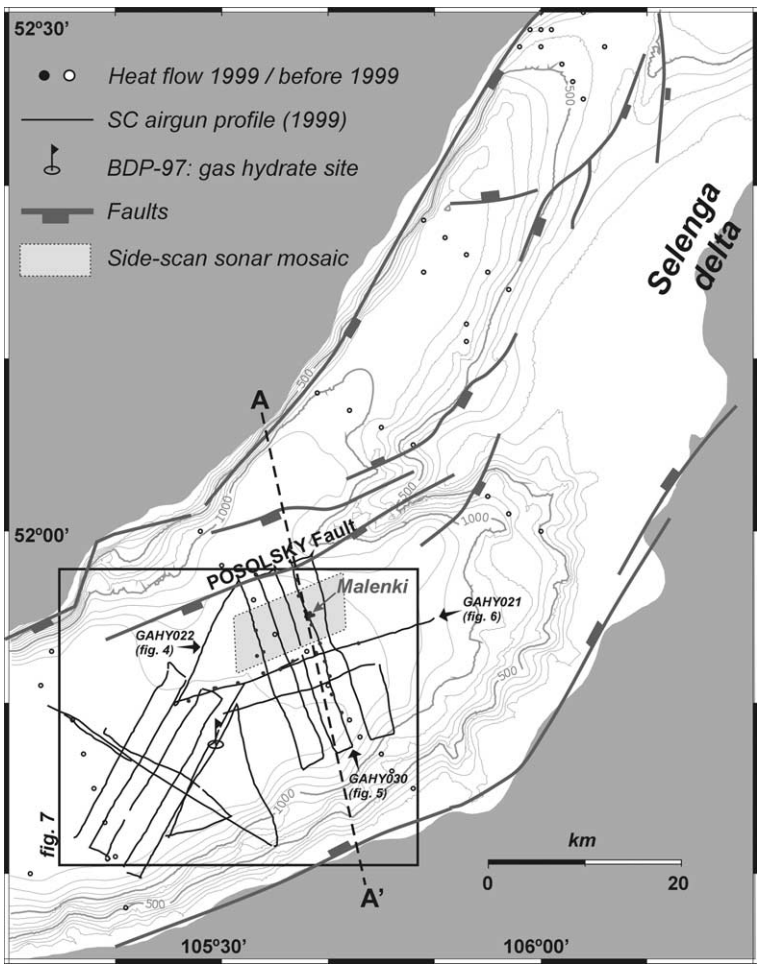

Fig. 2. Structural and bathymetric map of the SBB and the study area (black box, also shown in Fig. 7). In this study, we combine results from heat-flow measurements (dots) and SC airgun seismic reflection data (black lines). The grey zone represents the side-scan sonar mosaic, discussed in depth in Van Rensbergen et al. (2002). The line AA′ marks the cross-section of the SBB shown in Fig. 10. We also indicated the seismic data (GAHY021, GAHY022, GAHY030) shown in this paper and the location of the *Malenki* seep along line GAHY030.

in the area, but not at the borehole location itself (Vanneste et al., 2001). Hydrates saturated ~10% of pore space, and the clathrated gas was mainly methane (>99%) of biogenic origin (Kuzmin et al., 2000a). In March 2000, hydrates were retrieved from the uppermost sediment section in a 500 m wide low-relief crater and active venting site named *Malenki* (N51°55.8′-E105°38.0′ ±18 km away from the deep drilling site; Fig. 2) (Van Rensbergen et al., 2002).

Since hydrates were inferred in the Lake Baikal subsurface, their distribution in relation to heat-flow has been a point of strong interest. Golmshtok et al. (2000) discuss the relation between heat-flow and sub-bottom depths of the BSR based on the heat-flow data set acquired earlier by Golubev (1982). However, these studies dealt with generalised heat-flow features only, and disregarded small-scale variations mainly because of the sparse distribution of heat-flow data along specific tracks across the lake basins. Detailed contouring of heat-flow from the Northern Baikal Basin (NBB) revealed that such small-scale variations can be important (Golubev & Poort, 1995). In our study area, the reflection at the BHSZ exhibits anomalous behaviour. It expresses both undulations and lateral discontinuities. The recent discovery of methane gas venting sites (Van Rensbergen et al., in press) and accurate mapping of the BSR, gas related reflections (enhanced reflections, ER), and heat-flow variations (Vanneste, 2000) allowed us to compare the measured and inferred heat-flow values in relation with hydrate distribution.

The objectives of the paper are the following:

1. To present a new data set consisting of SC airgun profiles and heat-flow measurements along these profiles.
2. To discuss the different seismic features related to gas hydrates and/or free gas accumulation in a zone of seepage and faulting and illustrate the different modes by which gas hydrates may occur in this area.
3. To analyse and discuss the lateral changes of heat-flow and hydrate/free gas distribution inferred from seismic data and their correlation.
4. And to propose a possible link between laterally irregular hydrate distribution, fluid venting and the variable heat-flow characteristics based on fluid convection cells.

2. Geological setting

2.1. Lake Baikal

Lake Baikal is the world's deepest (CBB: 1637 m) and most voluminous lake (23,000 km^3), containing approximately 20% of the world-wide reserve of fresh water (salinity 0.76‰). The three lake basins SBB, CBB and NBB are highly asymmetric half-grabens with steeply dipping border faults on the western side, and they occupy the central part of the tectonically active Baikal Rift Zone (Logachev, 1993; Zonenshain, Kuzmin, Natapov, & Page, 1990) (Fig. 1). Two fault-controlled structural highs separate the lake basins: the *Selenga Delta Accommodation Zone* between the CBB and SBB and the *Academician Ridge Accommodation Zone* between the NBB and CBB. The Selenga Delta is underlain by a complex of deformed basement blocks. Cross-rift fault zones disrupt the generally flat basin floors. One of the most important structural features in the eastern part of the SBB is the *Posolsky Bank*, a thickly sedimented basement ridge, trending NE, obliquely to the main border fault and belonging to the Selenga Delta accommodation zone (Scholz & Hutchinson, 2000). This structure is bounded at the SE by a steep slope corresponding to the active *Posolsky fault* zone with a vertical displacement of more than 1 km (Klerkx, Hus, De Batist, Van Rensbergen, & Poort, 2000) (Fig. 2).

Results from deep drilling in the area of interest (BDP-97) demonstrate that turbidite deposition is the dominant sedimentation process in the deep SBB (Kuzmin et al., 2000b). Sedimentation rates derived from core analyses vary between 30 and 70 cm/ka with maximum values of 120 cm/ka in front of the Selenga Delta, where sediments are enriched in organic carbon content (Edgington et al., 1991). The thickness of sediments deposited since the Late Cretaceous is variable but can exceed 8 km (Mats, 1993; Zonenshain, Golmshtok, & Hutchinson, 1992). Within the seismic facies, a major transition occurs between a lower Oligocene to early Pliocene unit and an upper middle Pliocene to Recent unit, corresponding to a two-stage rifting mode (Logatchev & Florensov, 1978) related to changes in the paleostress field (Delvaux et al., 1997). The first, or *slow-rifting* stage initiated in the Oligocene (~30–35 Ma BP) and sustained for over 20 Ma with slowly subsiding basins. From mid-Pliocene times onwards, a strong acceleration in basin subsidence and flank uplift took place, referred to as the major phase of rifting or *fast-rifting stage*. While the former resulted in the deposition of mainly fine-grained sediments, the latter phase is dominated by coarser sediment input (Keller, Bott, Wendlandt, Doser, & Morgan, 1995). Hutchinson et al. (1992) provide evidence that this fast-rifting phase could be divided into two sub-phases with transition at the beginning of the Quaternary.

The Baikal Basins are also characterised by a complex pattern of active fault zones, and in relation to that, a highly variable heat-flow. Over the years, hundreds of heat-flow measurements were taken in the upper meters of the sediments of Lake Baikal (Golubev, 1982; Lubimova, 1969; Poort, 2000; and others). Measured heat-flow in the Baikal Basins varies between 40 ± 6 and 195 ± 25 mW/m^2 (mean value of 71 ± 21 mW m^{-2}). On smaller scale (order of km), heat-flow fluctuations with a magnitude of 30–40 mW/m^2 occur frequently. Local high positive heat-flow anomalies with magnitudes of more than 200–1000 mW m^{-2} have been observed along the regional border faults in the NBB. These anomalies are related to hydrothermal activity, as evidenced at the Frolikha Bay anomaly (Crane, Hecker, & Golubev, 1991; Golubev, Klerkx, & Kipfer, 1993). More than 50 hot springs have been documented on the shores of the Baikal Rift Basins (Pinneker & Lomonosov, 1973). Golubev (1990) suggested that all heat-flow anomalies in Lake Baikal can be attributed to ground water penetrating beneath the rift shoulders and rising as thermal waters along fault zones. Such a regional heat and fluid circulation by groundwater has shown to be feasible by numerical modelling studies (Poort & Polyansky, 2002).

2.2. Focus on the study area

The study area lies at the northern end of the axial part of the SBB (Figs. 1 and 2), in the hanging wall (south) of the Posolsky fault zone. The basin floor dips gently from 1340 to 1420 m towards the SW. Part of the study area is imaged by 30 kHz side-scan sonar and shows a variety of features discussed by Van Rensbergen et al. (2002). One of the features is a continuous antithetic undulating fault structure running in a NE–SW direction. This fault offsets the lake floor by up to 30 m, an effect that diminishes towards the NE, as seen on seismic profiles crossing this fault. It splits up in NE and SE trending splays, respectively. Also, four isolated semi-circular lake floor anomalies (craters and cones) with variable reflectivity are recognised, lining up nearly parallel to the antithetic fault. They have a diameter up to 800 m. Echo-sounding revealed the presence of 10–25 m high non-transparent plumes in the water column just above these structures, which are interpreted as active fluid seeps. The central part of the lake floor irregularities is depressed. The irregularities are interpreted to be recent mud volcanoes or craters and may be related to active hydrate destabilization (De Batist et al., 2002). During the 1999 expedition, 12 CTD casts were taken. These returned a mean bottom-water temperature of 3.36 ± 0.01 °C in the study area.

The main part of this paper discusses two seismic profiles along which several heat-flow measurements were taken. One of these lines GAHY030 crosses the antithetic fault structure almost perpendicularly, and touches one of the venting structures, the *Malenki* seep. The other seismic profile GAHY021 is located south of the area surveyed by side-scan sonar (Fig. 2). A few

heat-flow stations were deployed on another venting structure, called *Bolshoy*. These lie off the seismic tracks.

3. Data acquisition and methods

3.1. Seismic reflection profiling

The SC seismic data presented in this study were acquired in 1999 with a single 3 l Impuls airgun source. Sampling interval was 0.5 ms. Frequency content of this system ranges from 45 to 330 Hz. Shot interval was 16 s, resulting in an average shot spacing of ~30 m. The average penetration exceeds 500 ms two-way travel time (TWTT). The high-resolution SIG streamer unit was deployed in nearly zero-offset mode and towed at the water surface. The streamer has an active length of 2.7 m, containing 10 hydrophones with 0.3 m spacing. The signal is pre-amplified in the streamer.

Data processing included trace editing, true amplitude recovery and band-pass frequency filtering (50–250 Hz). Additionally, we performed attribute analyses for reflection strength, frequency, phase, and polarity in order to analyse the nature of the reflections. Lake floor and BHSZ reflection arrival times were picked interactively in Landmark ProMAX software for a maximum of traces.

3.2. Heat-flow measurements

During the third leg of the 1999 expedition, 23 heat-flow measurements were conducted, using the 2 m long GEOS-T thermoprobe (Table 1). The instrument is constructed according to the violin-bow design. Two sensor strings are used to measure the in situ thermal conductivity and temperature at the lake floor and from four depth intervals of 0.5 m. The thermal conductivity probe contains a linear heat element in combination with four grouped thermistors. Conductivity is then determined using the continuous heating technique (Lister, 1970). The instrumental error is 0.002 °C m^{-1} on the geothermal gradient determined between two temperature data points and about 5% on the thermal conductivity measured. On top of the probe, a thermometer and bathometer record the bottom-water temperature and the water depth, respectively. Dip angle of the probe is also registered with an accuracy of 1°. All geothermal data were logged at 2.5 s intervals. Real-time monitoring during probe lowering allows controlling the instrument performance and the data quality. Probe leakage and failure or incomplete penetrations due to hard substrate or dipping seafloor are easily evaluated. In stations where thermal conductivity measurements were not successful, we replaced these by the values measured in neighbouring stations.

We selected the heat-flow stations based on the information from previously acquired seismic and side-scan

Table 1
Heat-flow data acquired during the 1999 Lake Baikal expedition

Station	Location	Latitude (N)	Longitude (E)	H (m)	#	G (mK/m)		k (W/m/K)		q (mW/m)	
HFA03	Malenki	51°55.146′	105°38.406′	1316	5	102	7	0.75	0.04	76	7
HFA04	GAHY030	51°57.175′	105°37.017′	1292	4	78	6	0.99	0.09	78	7
HFA05	GAHY030	51°56.276′	105°37.251′	1329	5	86	9	0.86	0.09	74	6
HFA06	GAHY030	51°55.397′	105°37.867′	1332	5	86	6	1.04	0.04	89	9
HFA07	GAHY030	51°54.612′	105°38.456′	1317	5	86	7	1.03	0.13	89	4
HFA08	GAHY030	51°53.534′	105°39.250′	1341	5	67	4	0.89	0.08	60	8
HFA11	Malenki	51°54.934′	105°38.209′	1317	5	92	6	0.88	0.08	82	7
HFA12	Malenki	51°55.167′	105°38.300′	1311	2	180	–	0.91[a]	–	165	–
HFA13	Malenki	51°55.292′	105°38.303′	1317	3	102	4	1.11	0.04	113	8
HFA14	Malenki	51°55.122′	105°38.392′	1317	5	93	4	0.92	0.12	86	8
HFA15	Malenki	51°55.166′	105°38.617′	1322	5	102	7	0.91	0.05	92	4
HFA16	GAHY030	51°55.075′	105°37.947′	1316	5	83	7	0.97	0.12	81	12
HFB01	GAHY021	51°53.542′	105°42.870′	1319	4	96	6	0.94	0.05	90	1
HFB02	GAHY021	51°53.005′	105°38.890′	1354	3	71	14	0.89[a]	–	63	–
HFB03	GAHY021	51°52.520′	105°36.708′	1369	5	82	13	0.97	0.14	79	3
HFB04	GAHY021	51°52.044′	105°35.501′	1390	4	91	6	0.92	0.10	84	6
HFB05	GAHY021	51°51.826′	105°33.900′	1390	3	93	6	0.90	0.04	84	2
HFB06	GAHY021	51°51.267′	105°31.525′	1411	5	72	16	1.00	0.10	71	13
HFB08	GAHY021	51°50.232′	105°26.886′	1423	5	74	3	0.82	0.03	61	2
HFB09	GAHY021	51°50.960′	105°29.438′	1422	5	96	2	0.75	0.02	72	2
HFC01	Bolshoy	51°52.819′	105°33.319′	1365	5	101	9	1.09	0.12	111	14
HFC02	GAHY023	51°54.292′	105°33.207′	1373	5	90	7	0.83	0.05	75	8
HFC03	GAHY023	51°53.045′	105°33.931′	1365	4	95	9	0.93	0.13	90	21

H, water depth; #, number of thermistors; G, measured geothermal gradient; k, in situ thermal conductivity; q, calculated averaged heat-flow value, and standard deviations for the respective parameters.

[a] The thermal conductivity measurement failed, in which case the value of the nearest neighbouring station is adopted.

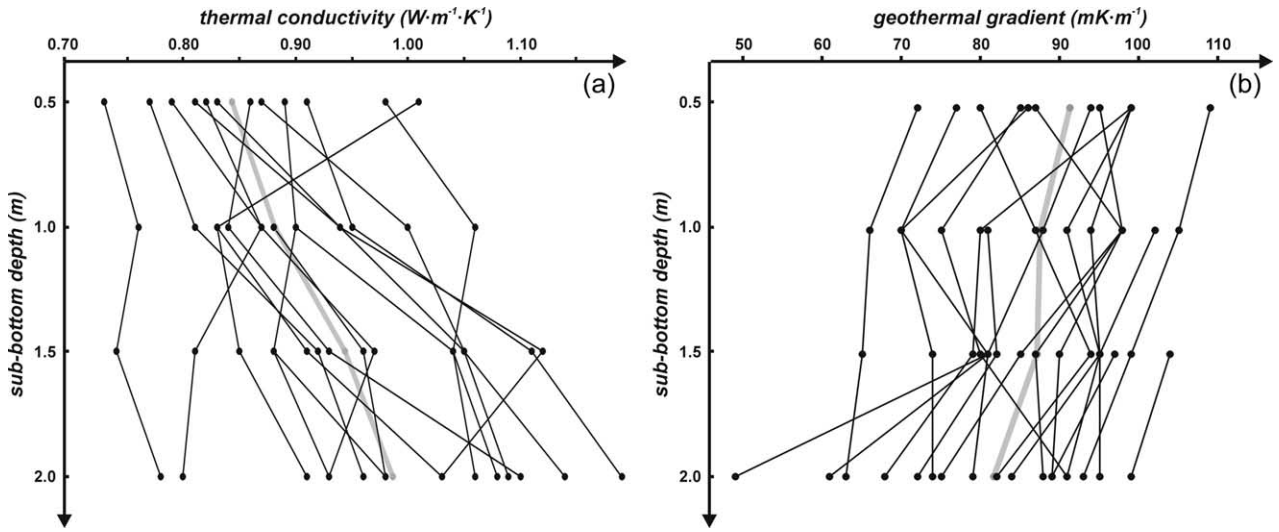

Fig. 3. Thermal conductivity (a) and geothermal gradient (b) with depth for all heat-flow stations (Table 1), as an illustration of their quality. The bold grey lines represent the average values for each depth.

sonar data. Stations were basically chosen along line GAHY030 and in the immediate vicinity of the *Malenki* seep (series HF-A) and along GAHY021 (series HF-B). Another three stations were taken in the *Bolshoy* crater (series HF-C). At each station, a mean thermal gradient, a mean conductivity, and their respective standard deviations were calculated (Table 1). In case a strong break is observed, the geothermal gradient is rejected or determined with a reduced number of in situ temperature values. At most stations, thermal conductivity increases slightly with depth (Fig. 3a), from 0.84 ± 0.09 W K^{-1} m^{-1} near the seafloor to 0.99 ± 0.12 W K^{-1} m^{-1} at 2 m depth. Such behaviour is commonly observed in the uppermost sediments and is interpreted to result from sediment compaction with burial depth. As a result, geothermal gradient values slightly decrease with burial depth (Fig. 3b), from 91.3 ± 11.1 mK m^{-1} at the first sampling interval to 81.6 ± 14.9 mK m^{-1} at 2 m sub-bottom depths. Heat-flow values are then computed for each interval depth as the product of the geothermal gradient and the thermal conductivity, and then averaged for each station. The calculated heat-flow ranges from 60 to 165 mW m^{-2} (Table 1).

Especially in the upper part of the sedimentary column, environmental effects can alter the measured heat-flow values significantly. Hence, the data coming from the 2 m thermoprobe have to be interpreted with caution. In addition to the instrumental error, heat-flow measurements are also sensitive to a number of geological and hydrological factors (Sundvor, Eldholm, Gladczenko, & Planke, 2000), e.g. sedimentation, sea floor or lake floor topography and dipping, bottom-water instability, heat refraction, erosion, uplift, etc. Corrections for regional topography and sedimentation using simplified models (van Herzen & Uyeda, 1963; Lachenbruch, 1968) are estimated to be less than −5 to 10% of the measured values. Also, seasonal bottom-water temperature variations should be taken into account, since they can affect geothermal gradient values, and hence heat-flow. Bottom-water temperatures in Lake Baikal can change by ~0.1 °C (Golmshtok et al., 2000), but this is variable from year to year and from place to place. Unfortunately, we do not have a detailed data set for our study area. The summer bottom-water temperature measured with the CTD casts (see earlier) show that the bottom-water temperatures are uniform in the study area. The individual temperature data points show a reasonable trend in the uppermost 2 m of sediments (Fig. 3). This trend illustrates that, at the relatively deep setting of the study area, such bottom-water temperature changes are most probably limited.

3.3. Inferred heat-flow and its accuracy

The presence of BSRs has often been used to estimate the geothermal field in different geological settings (Bangs & Brown, 1995; Bouriak, Vanneste, & Saoutkine, 2000; Grevemeyer & Villinger, 2001; Yamano, Uyeda, Aoki, & Shipley, 1982). The procedure assumes that the BSR coincides with the three-phase methane hydrate–fresh water–methane vapour boundary, and consists of the following steps (Appendix A):

1. Conversion from TWTT to sub-bottom depths based on the velocity model derived from MCS data for Lake Baikal (Golmshtok et al., 2000).
2. Calculation of in situ hydrostatic and lithostatic pressure.
3. Derivation of the equivalent three-phase methane hydrate equilibrium temperature for these pressure values at the inferred BSR depth, using an analytical phase boundary equation.
4. Determination of the geothermal gradient and heat-flow.

In our comparison of inferred and measured heat-flow, we used the raw heat-flow values.

Accuracy of inferred heat-flow depends on all parameters in the methodology. Gas hydrate equilibrium conditions were determined using the program CSMHYD (Sloan, 1998) for pure methane hydrates (>99%) in a fresh water environment. The very low salinity of the Baikal waters (0.76‰) does not shift the equilibrium conditions from pure fresh water significantly. However, deviations from the vapour phase composition (addition of minor amounts of CO_2, N_2 or C_2H_6), gives rise to slightly higher inferred heat-flow of the order of 2%. Inferred heat-flow is more sensitive to additions of C_3H_8 and H_2S, but the propane concentration was too low (<0.1%) to result in noticeable deviations and there was no evidence of H_2S in the hydrate samples.

Another factor of importance is the sub-bottom velocity profile used, and the influence of partial hydrate saturation on the interval velocity, and hence sub-bottom depth of the BHSZ. Modelling of the weighted equation (Lee, Hutchinson, Collett, & Dillon, 1996) for disseminated hydrate distribution (Tinivella, 1999), assuming a maximum of 30% hydrate saturation of pore volume in a limited interval above the BHSZ, results in inferred heat-flow values that are only slightly lower (5%) than in the hydrate-free case, although the interval velocity profile is significantly different (Vanneste, 2000). This effect is more or less ruled out since the ratio is taken between equilibrium temperature and sub-bottom depths for calculating the geothermal gradient. Bulk density changes due to gas or gas hydrate presence are very small as well.

The factor of highest uncertainty is the thermal conductivity profile with depth, since this one is only available for the first 100 m of sediments (Duchkov & Kazantsev, 1996) and is extrapolated to deeper parts of the sedimentary section, ignoring the effect of partial hydrate saturation of pore volume. Note that the average sub-bottom depth of the BHSZ is about 300 m in the study area.

Summarised, the overall accuracy of inferred heat-flow measurements presented is estimated to be 15%, but the relative accuracy is better.

4. Gas hydrates, free gas accumulation and heat-flow variability

4.1. Seismic evidences for shallow gas accumulations and gas hydrates

A typical example of a common BSR feature is observed on line GAHY022 (Fig. 4). This BSR clearly cross-cuts the stratigraphy and has reversed reflection polarity relative to the lake floor reflection. Its position mimics more or less the topography of the lake floor. Its reflection amplitude is not very strong and laterally variable. Above the BSR, the reflection amplitudes seem reduced, but this cannot be unambiguously attributed to partial hydrate saturation. Beneath the BSR, some enhanced reflections occur, suggesting that free gases accumulate only within specific strata. The BSR also crosses some small-offset normal faults that apparently do not severely disrupt the BSR's continuity. Nevertheless, some enhanced reflections are present within the suspected HSZ, illustrating localised gas migration/presence. The BSR disappears within the structural high (NE).

Rather different and surprising features are observed on the seismic lines running nearly perpendicular to the antithetic fault. One of these unique profiles (GAHY030, Fig. 5a) crosses the *Malenki* seep. A dipping reflection is present at the SSE part of the profiles. This anomalous reflection loses its continuity close to the antithetic fault

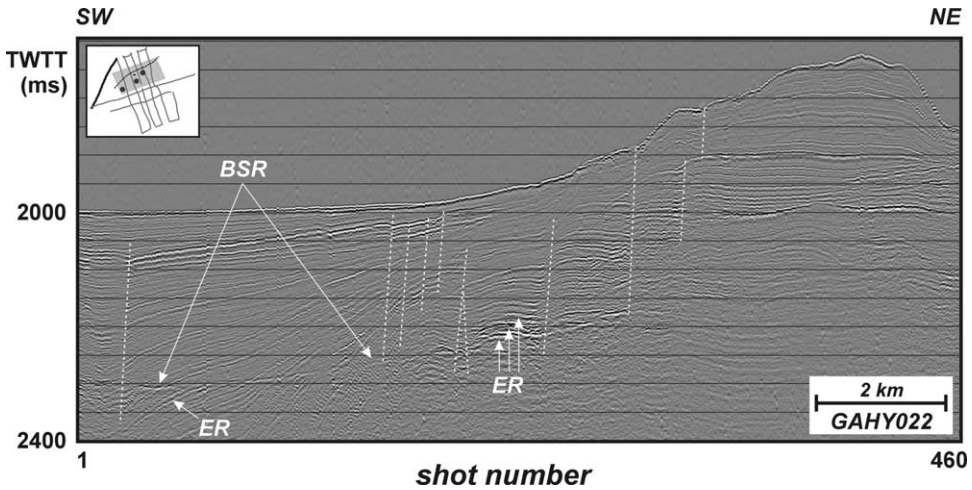

Fig. 4. SC airgun-line GAHY022 from the SBB with evidence of a cross-cutting BSR feature. The BSR disappears within the structural high on the NE side of the seismic profile. Note that the reflection amplitude is weak and laterally variable. Some enhanced reflections are present just above the BSR and might indicate the local presence of free gas within the HSZ. The inset shows the location of the seismic profile (bold line) relative to the fluid escape features (dots), side-scan sonar mosaic (grey shading), and antithetic fault structure (dashed line).

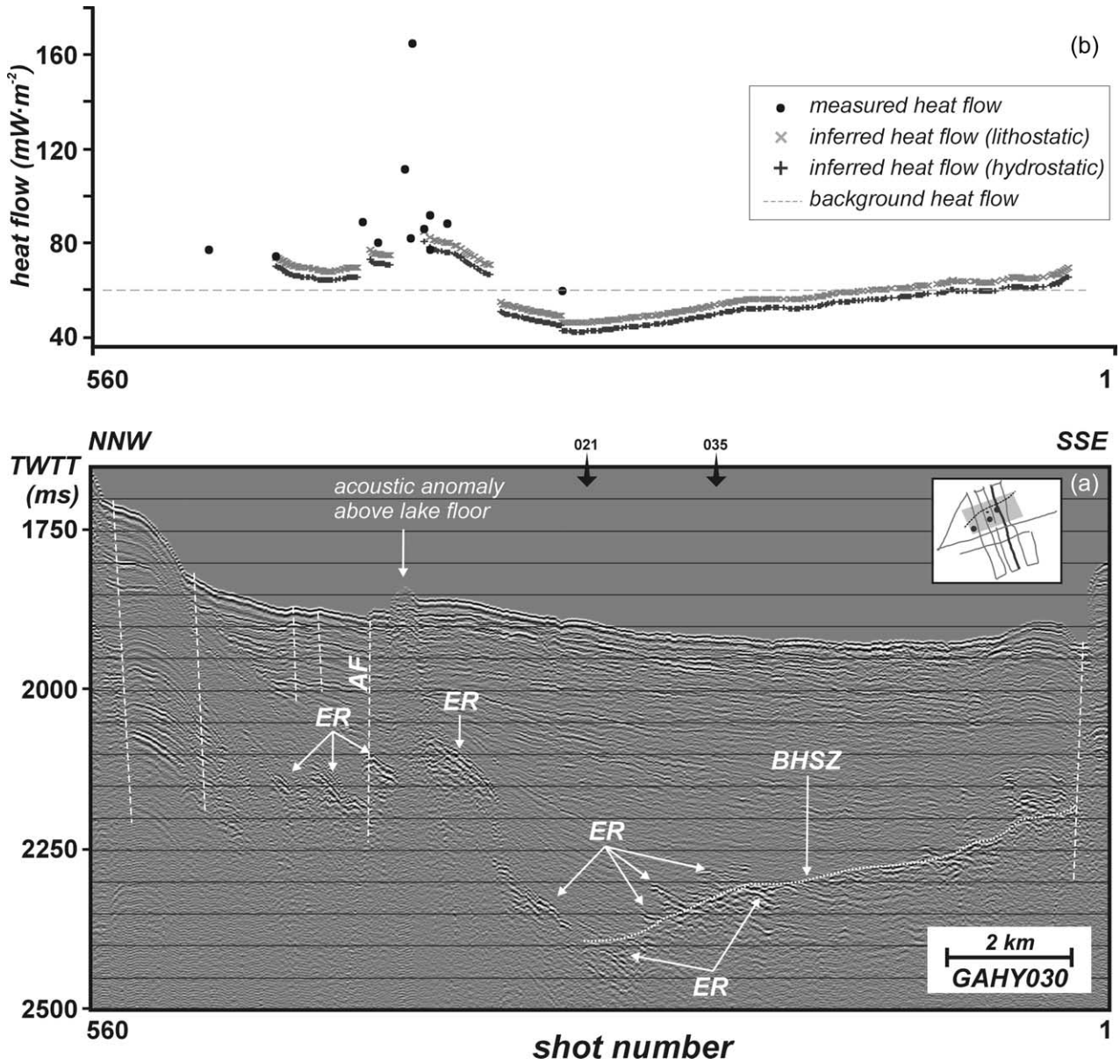

Fig. 5. (a) SC airgun-line GAHY030 crossing the *Malenki* crater, showing remarkable changes of the BHSZ in the immediate vicinity of the seepage. An antithetic fault (AF) offsets the lake floor. The inset shows the location of the seismic profile (bold black line) relative to the fluid escape features (dots), side-scan sonar mosaic (grey shading), and antithetic fault structure (dashed line). (b) Measured and inferred heat-flow values along line GAHY030 (see (a)) showing an overall good correlation. Measured heat-flow exceeds inferred one. Inferred heat-flow is calculated using both hydrostatic and lithostatic pressure approach.

zone, where it is replaced by a series of enhanced reflectors appearing at variable sub-bottom depths. A columnar disturbance or acoustic chimney interrupts the stratigraphy up to the lake floor. It corresponds to the *Malenki* mud crater, and is explained in terms of gas escape—temporary or continuously—and/or elevated heat-flow caused by seepage from the sub-surface resulting in acoustic attenuation. Similar features have been reported from other areas worldwide (Hovland & Judd, 1988; and references therein). The high attenuation makes it impossible to localise the zone from where the fluids or source material are mobilised. Some enhanced reflections terminate at the sides of this feature and the northern antithetic fault splay. These bright spots have a very high reflection strength, and negative apparent polarity. No coherent BSR feature can be observed at the NNW side of the antithetic fault structure, although some very faint and short cross-cutting BSR-like features and bright spots can be recognised. At some locations, enhanced reflections penetrate the HSZ from below. The parallel seismic profiles show similar characteristics with an undulating reflection, which does not mimic the lake floor reflection.

Profile GAHY021 (Fig. 6a) lies a few km south of the fluid escape structures and the antithetic fault, and shows yet

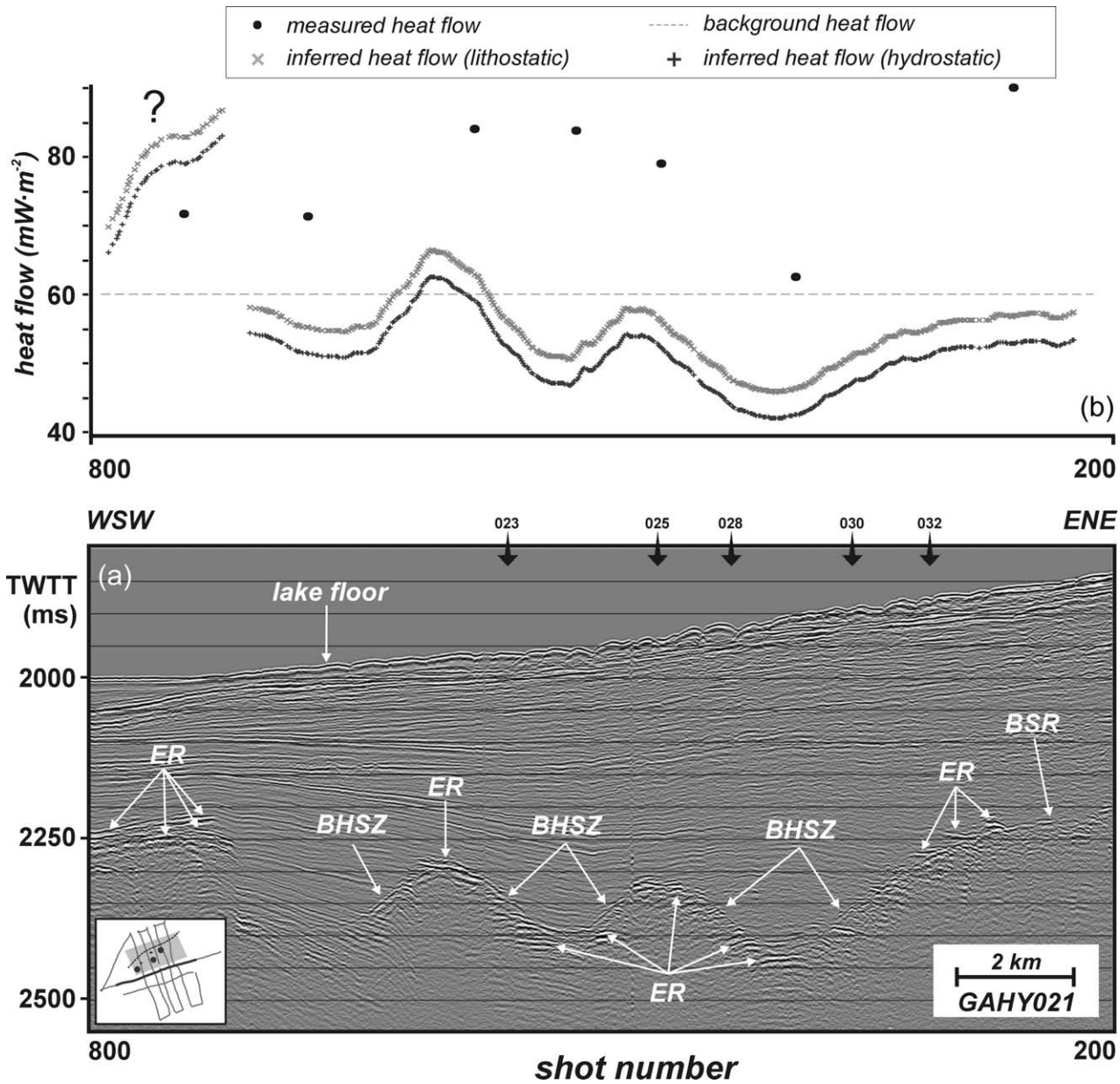

Fig. 6. (a) SC airgun-line GAHY021 characterised by a high-amplitude undulating and reversed polarity reflection that cross-cuts the local stratigraphy and hence is attributed to the gas hydrate-free gas interface. Note that some enhanced reflections penetrate the BHSZ, suggesting percolation of free gases within the HSZ. The inset shows the location of the seismic profile (bold black line) relative to the fluid escape features (dots), side-scan sonar mosaic (grey shading), and antithetic fault structure (dashed line). (b) Measured and inferred heat-flow values along line GAHY021 (see (a)). Contradictory to observations on Fig. 5, the correlation between inferred and measured heat-flow is poor. Measured heat-flow is significantly higher than inferred heat-flow. Inferred heat-flow is calculated using both hydrostatic and lithostatic pressure approach.

another atypical reflection. This line coincides with the low-resolution image presented in Golmshtok et al. (2000). Along this line, a cross-cutting high-amplitude, but oscillating reflection, of reversed polarity, marks the BHSZ. This undulating behaviour occurs completely independent of the slightly dipping lake floor. The total sub-bottom difference between the lows and the highs taken from this line ranges from about 100 ms (e.g. shot points 395 and 470) to about 250 ms TWTT (shot points 395 and 600). The oscillation wavelength is only a few kilometres. This seismic section does not show evidence of vertical fluid migration pathways, as observed on line GAHY030 (Fig. 5a). This anomalous undulating behaviour disappears to the ENE, where it is converted into a bottom-mimicking feature. The main reason why the BHSZ image is less pronounced than on the low-resolution airgun data, is the higher frequency content of the acoustic source used, as shown in Vanneste et al. (2001).

At the intersection of both lines, the oscillating BHSZ reflection (GAHY021, Fig. 6a) matches perfectly with the irregular reflection (GAHY030, Fig. 5a), indicating that these two uncommon reflections have the same nature or

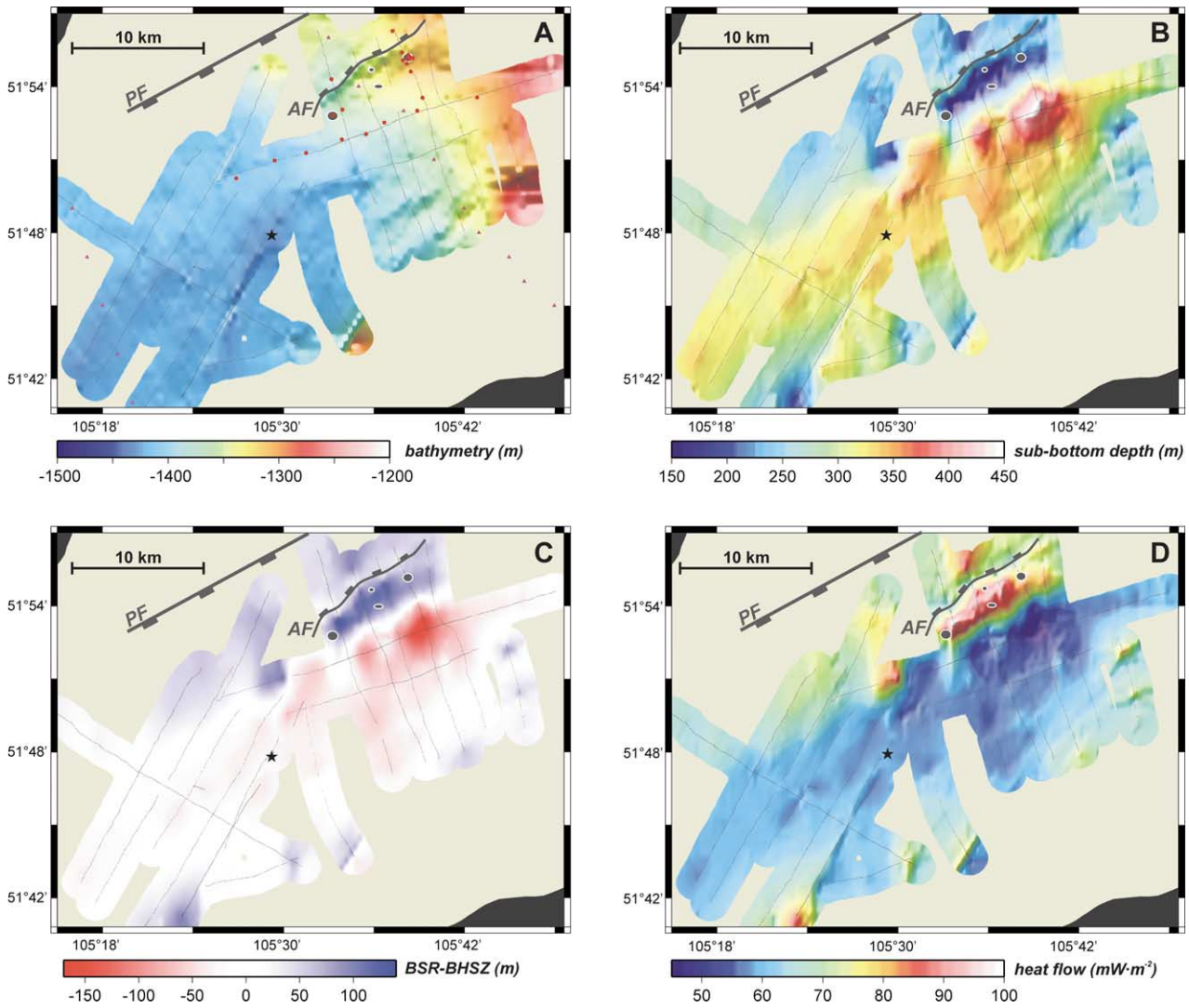

Fig. 7. (a) Illuminated bathymetry, (b) illuminated BHSZ sub-bottom depths, (c) difference plot of theoretically expected BSR sub-bottom depths and observed BHSZ sub-bottom depths and (d) inferred heat-flow in the study area, from inversion of seismic data. The red circles (a) are heat-flow stations from 1999, the purple triangles (a) are heat-flow data compiled by Golubev (1982). The dark circles represent mud volcanoes. Data further away than 1.5 km from sampling point are masked. PF, Posolsky fault; AF, antithetic fault. Maps were generated with GMT (Wessel & Smith, 1991).

origin, but with a different expression along the two profiles. With the exception of the non-bottom-simulating behaviour, these reflections express all typical characteristics of a common reflection at the BHSZ as observed in other hydrate provinces world-wide, the BSR feature observed in Fig. 4, the seismic data just ESE of the side-scan sonar mosaic and further away from the fluid escape structures (Vanneste, 2000; Vanneste et al., 2001): (1) the reflections have negative apparent reflection polarity, (2) the reflections obliquely cut the stratigraphy, (3) spectral analyses performed in a 100 ms window just above and just beneath this reflection, and averaged over 500 neighbouring traces, reveal a drop in peak frequency from 150 to 110 Hz, (4) the reflection strength of the reflection is laterally variable, but often enhanced compared to reflections of lithological boundaries, (5) often, enhanced and polarity-reversed reflections occur just below the reflection, (6) AVO analyses were performed on the multi-channel counterpart of line GAHY021 and show an increasing reflection amplitude with offsets (Vanneste, 2000; Vanneste et al., 2001). Hence, we interpret this unique feature as the interface between partially hydrate saturated sediments above and gas-containing sediments beneath. These phenomena are then attributed to free gas presence beneath the BHSZ. The reflection at the BHSZ or the top of the free gas zone does not need to be a BSR in the strict sense of the word. This is clearly illustrated in Fig. 7, where we compared the bathymetry (Fig. 7a) and BHSZ (Fig. 7b) extracted from the seismic data discussed (see later).

4.2. Heat-flow data and local variability

Heat-flow varies significantly in the study area. The measured heat-flow ranges from 56 to 165 mW m^{-2}

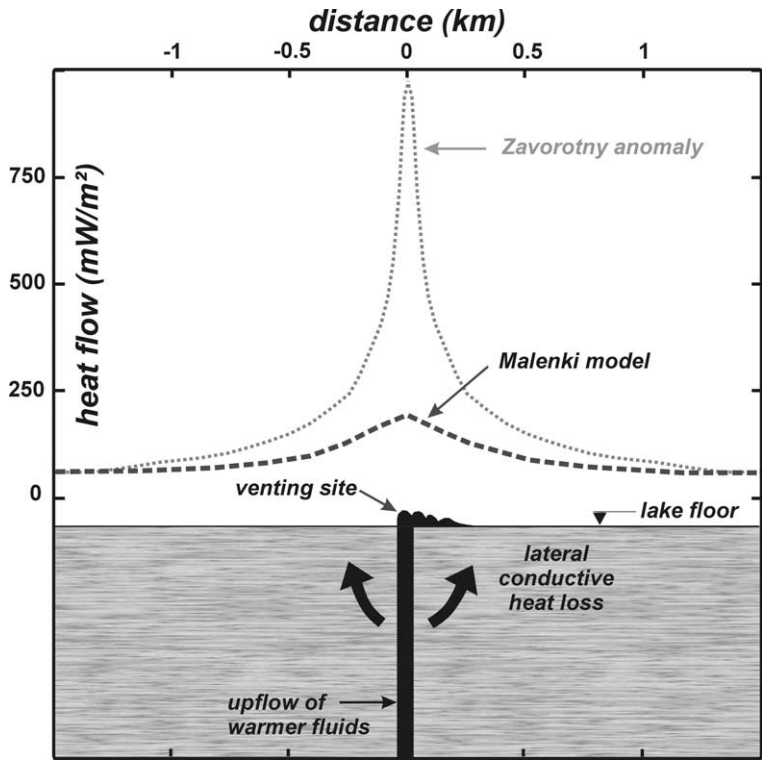

Fig. 8. Comparison of the modelled heat-flow trend across an active seep structure, typical for the NBB, and the heat-flow pattern as measured along GAHY030 over the *Malenki* crater.

(Table 1). The highest values are recorded at or in the immediate vicinity of the venting sites: 113–165 mW m^{-2} for *Malenki* and 111 mW m^{-2} for *Bolshoy*. Excluding these exceptionally high values, the mean heat-flow in the study area is 77.5 ± 10.8 mW m^{-2}, i.e. slightly higher than the average heat-flow in the SBB. Such high heat-flow and strong variability are local phenomena, which is also illustrated by comparing these values with heat-flow data acquired previously in the surrounding area (Golubev, 1982).

In order to explain such local heat-flow variability, several factors should be considered. The instrumental error (~10%) can be ruled out. We already mentioned the environmental processes that can disturb near surface heat-flow in the study area above. Bottom-water temperatures appear to be stable, and the errors related to sedimentation and topography can account for changes between −5 and +10% of the raw heat-flow values listed. These estimates suggest that environmental aspects have only a limited effect on the heat-flow values, and more important, such effects are regional, and hence not suitable to explain the local variability of the heat-flow pattern as observed. Taking this into consideration, then the most plausible explanation for the variability of heat-flow has to be found in local fluid advection or circulation processes.

Side-scan sonar evidence of several active fluid discharge structures in the study area interpreted as recent mud volcanoes and active methane vents (Van Rensbergen et al., 2002) supports this reasoning. The best control from our data set comes from the *Malenki* crater area, where heat-flow measurements vary between 55 and 110 mW m^{-2}, with one additional extreme of 165 mW m^{-2} at the core of the seepage structure. Most probably, part of the heat-flow variability results from the presence of fluid flow. By plotting the heat-flow data across the venting site (Fig. 8), we observe a similar curve like those observed from the heat-flow anomalies in the NBB (Golubev & Poort, 1995). As modelled for the Zavorotny anomaly in the NBB (Poort, 2000), such surface heat-flow expression can result from the focused upflow or warmer fluids along a permeable conduit or pathway. The intensity of the *Malenki* seep is significantly smaller than the hydrothermal vents documented in the NBB, where heat-flow anomalies of 1–10 W m^{-2} are not exceptional.

5. Inferred vs. measured heat-flow

5.1. Heat-flow trends along GAHY030 and GAHY021

The first series of heat-flow measurements (HF-A, Table 1) was taken along line GAHY030 (Fig. 5a). The seismic profile and the correlation between measured and inferred heat-flow for both hydrostatic and lithostatic pressure conditions are shown in Fig. 5b. The reflection interpreted as the BHSZ follows the heat-flow trends with discrepancies of less than 15%, i.e. within the estimated accuracy of the methodology. Measured heat-flow exceeds

the inferred heat-flow along the entire profile. Inferred heat-flow reaches maximum values close to the acoustic chimney (82–86 mW m^{-2}) in the same order of magnitude as the heat-flow measurements (82–92 mW m^{-2}). Two heat-flow stations gave higher values of 113–165 mW m^{-2}, but these occur within the seep structure where no clear BHSZ reflection is observed (columnar disturbance, Fig. 5a). The lowest heat-flow values occur a few km SSE from the venting sites, both inferred (45–49 mW m^{-2}) and measured (56 mW m^{-2}). Further to the SSE, inferred heat-flow values increase again (Fig. 5b) to 60–65 mW m^{-2}, returning to normal background values for this part of Lake Baikal. In this area, heat-flow measurements failed, due to poor penetration of the probe. Fig. 5b also shows that both the local highs and lows of the BHSZ or inferred heat-flow are atypical features with a local character. Nevertheless, the correlation between inferred and measured heat-flow is reasonable along this line, despite the presence of significant fluid discharge from the sub-surface.

The situation is different along line GAHY021 (Fig. 6a) and coinciding heat-flow stations (series HF-B, Table 1, Fig. 6b). Heat-flow correlation is rather poor, and deviations are much larger, approaching 40%, than along GAHY030. While measured heat-flow is high compared to the background values, the deduced heat-flow values are in general lower than the background values. Near the crossing point of lines GAHY021 and GAHY030 (see later), we measured a smaller heat-flow (63 mW m^{-2}). This value is exceptionally small compared to the other measured data along line GAHY021, but fits well considering the oscillating pattern in both measured and inferred data (Fig. 6b), and with the neighbouring heat-flow value measured along GAHY030 (Fig. 5b). The heat-flow maxima and minima of the data sets show the same trend along line GAHY021. One of the inferred lows is, however, not supported by the measurements. The overall large discrepancies between both data sets, the short-wavelength oscillating behaviour of the BHSZ and especially the deep burial of the BHSZ are not easily explained. Golmshtok et al. (2000) report the presence of fault structures, terminating beneath some of the local highs of the BHSZ reflection. These faults then serve as pathways for warmer water migrating from depth, and can in turn result in the shoaling of the BHSZ. We do not observe these fault structures beneath the BHSZ due to the limited penetration of the acoustic energy. Nevertheless, in our view, the presence of such faults cannot explain the presence of local BHSZ depressions. To the W of the seismic profile, a package of enhanced reflections is present. If these represent the BHSZ, then this area is the only zone where inferred heat-flow measurements exceed measured ones. However, we lack crossing seismic data to verify this.

5.2. Inferred heat-flow contours and zonation

The data shown above reveal extraordinary characteristics of both the lateral and vertical extent of the HSZ in the immediate vicinity of fluid escape features and intrabasinal faults. In Fig. 7 we show a set of structural contour maps extracted from the seismic data to further illustrate and analyse this. While the antithetic fault flanking the fluid discharge structures forms the only discontinuity or irregularity on the gently dipping bathymetry (Fig. 7a), the sub-bottom depth of the BHSZ (Fig. 7b) and hence inferred heat-flow (Fig. 7d) behaves significantly different and shows remarkable variability. The fluid discharge structures fall within a narrow zone of elevated heat-flow, most probably related to more intensive fluid migration through the faults and the mud volcanoes. This is confirmed by the heat-flow measurements showing similar small-scale variability (Fig. 7d). A broader zone of low to very low heat-flow or deep-seated BHSZ flanks this zone on the SSE. Fig. 7c expresses the anomalies in the same area, i.e. the difference between the expected BSR behaviour for a background heat-flow value of 60 mW m^{-2} and the observed BHSZ. This figure gives a better idea about the extent of the anomalous zones. We see that the regions of positive and negative anomalies are restricted to a small area surrounding the fluid escape structures. The SW part is free of anomalies, and corresponds to a zone of 'normal' BSR behaviour discussed by Vanneste et al. (2001).

5.3. Correlation and discrepancies

Based on the comparison of inferred and measured heat-flow along the two seismic sections GAHY021 and GAHY030 (Figs. 5b, 6b and 7), we conclude the following.

A first observation is that the inferred heat-flow values are in general lower than the measured ones. Differences are up to 40%, with the highest discrepancies observed along line GAHY021 characterised by the oscillating BHSZ reflection (Fig. 6b). Such anomalies clearly exceed the estimated errors on both methodologies. This also means that extrapolating surface heat-flow values to predict the in situ gas hydrate equilibrium temperature will show significant disparities, in general exceeding 5 °C. Thermal investigations from ODP Leg 164 (Blake Ridge) also revealed similar discrepancies of 30% between the inferred three-phase hydrate equilibrium temperature and the downward extrapolation of shallow geothermal gradients (Ruppel, 1997; Wood & Ruppel, 2000). However, deep temperature measurements along the borehole showed the opposite trend, i.e. lower than inferred temperatures at the BSR (Wood & Ruppel, 2000). As the authors state, it is quite striking that such anomalies occur in the Blake Ridge, which is a tectonically quiet passive margin with low advective flux. They fail to give a clear explanation.

The difference in Lake Baikal is that its basins occupy an active intracontinental tectonic rift basin, characterised by intensive faulting, high seismicity, and by lake floor fluid discharge. The new heat-flow data were all acquired in an area characterised by such faulting and associate fluid venting. This implies that convective/advective heat

transport cannot be ignored, and will contribute to measured heat-flow. As a result, the addition of an advective component will result in deviations from the pure conductive sub-bottom temperature profile in the sense that in situ temperature will be lowered taking a fixed (measured) heat-flow value (Davis, Hyndman, & Villinger, 1990; Xu & Ruppel, 1999). This will reduce the differences encountered. An example is given in Fig. 9 using the mean inferred heat-flow value of 58.7 mW m^{-2} over the study area and the average measured heat-flow of 77.5 mW m^{-2}, excluding the measurements in the active seeps (Table 1). The BHSZ then occurs at about 300 m sub-bottom depths. We constructed a series of extrapolated sub-bottom temperature profiles, using both a constant thermal conductivity (light grey curves) and a linear function with depth according to Duchkov and Kazantsev (1996) (dark grey curves), for pure conductive heat transfer (solid lines) and a combination of the conductive and advective heat transfer (dashed lines). This model illustrates that, for example, an advective flux of 7 mm yr^{-1} significantly reduces the extrapolated temperature differences at the depth of the inferred BHSZ. This is only a 1D model, ignoring that fluid flow patterns can be rather different near the surface than at depth, but it highlights the effect of fluid advection on extrapolated heat-flow values and their accuracy for hydrate equilibrium determinations. It is also worth noting that a study performed on the Makran Accretionary Prism showed an opposite discrepancy with BSR-derived heat-flow estimates exceeding measured ones (Kaul, Rosenberger, & Villinger, 2000).

An alternative explanation for the observed misfits may be that the BHSZ lies at non-equilibrium conditions. Non-equilibrium conditions at the BHSZ resulting from driving forces such as changing bottom-water temperatures and climatically and/or tectonically controlled lake level changes can be excluded because of the limited spatial extent of the zone of anomalies and their amplitudes. Another possibility is changes in the gas composition, as put forward to explain double BSRs on the Norwegian Margin (Posewang & Mienert, 1999). The authors state that it is questionable whether the gas composition and migration through a relatively uniform sedimentary section can change and what the cause could be. Preliminary analyses of the deep-seated hydrates (BDP-1997) in a zone of normal BSR behaviour and those retrieved from the *Malenki* mud volcano 18 km more to the NE are similar, further questioning this hypothesis. Other deviations may arise from porous medium or capillary effects (Clennell,

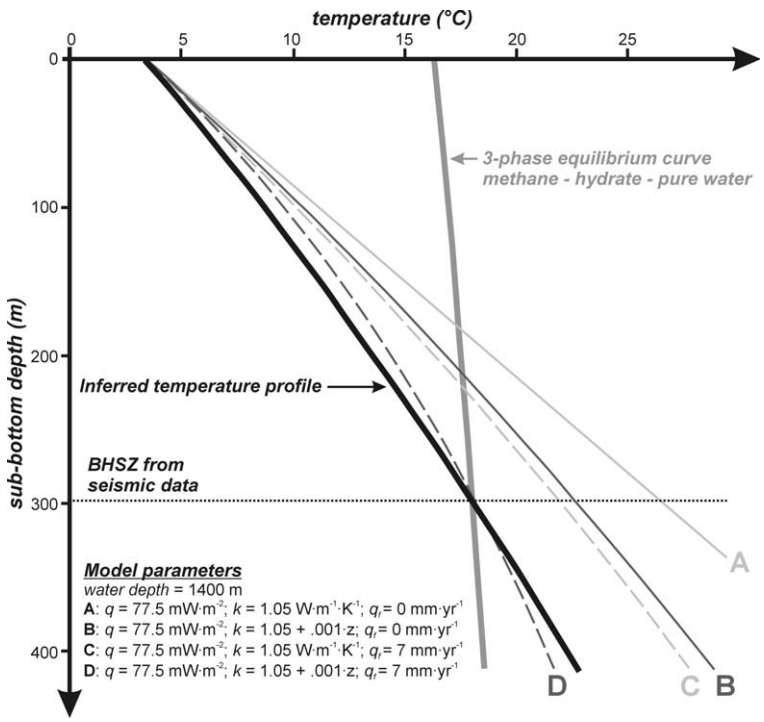

Fig. 9. Comparison between the inferred sub-bottom temperature profile (bold black line) based on the presence of a reflection at the BHSZ at an average of ~300 m sub-bottom depths and mean inferred heat flow of 58.7 mW m^2, and extrapolated temperature curves based on the mean shallow heat-flow measurements ($q = 77.5$ mW m^{-2}). The nearly vertical bold grey line represents the three-phase methane–water–hydrate boundary assuming hydrostatic pressure within the sediments for a water depth of 1400 m typical for the SBB. This figure clearly illustrates that extrapolating surface heat-flow measurements can result in overestimated temperatures at the depths of the inferred BHSZ. If part of the heat-flow comes from an advective fluid flux (q_f) additional to a conductive part, then the temperature differences at depths decrease. For the dashed curves, fluids are assumed to migrate vertically with a velocity q_f of 7 mm yr^{-1}. Note that the differences between these sub-bottom temperature profiles at 2 m depth, i.e. at the deepest part of the heat-flow probe, is only of the order of 0.04 °C.

Hovland, Booth, Henry, & Winters, 1999; Henry, Thomas, & Clennell, 1999; Ruppel, 1997). Finally, also lateral changes in methane or gas flux may result in different sub-bottom depths, where the BHSZ reflection is observed (Wood & Ruppel, 2000). Keeping this in mind, we consider neo-tectonic activity and fluid flow processes in the form of advection and circulation as the most likely candidates to explain the observed heat-flow discrepancies.

6. Discussion: fluid migration patterns in Lake Baikal and BSR disruption

6.1. Evidence of fluid migration

Methane migration in sediments can occur as a single pore fluid flow in which gases are dissolved into the rising pore water, as free gas bubbles driven by buoyancy or by molecular diffusion along concentration gradients (Ginsburg, 1998). Our data show abundant evidence for the migration and accumulation of free gas in the SBB on different scales. First of all, free gas is migrating to, or accumulating beneath, the BHSZ giving rise to the typical amplitude-enhanced and polarity-reversed reflections. Following this reasoning, the inferred presence of hydrates is considered indicative of fluid migration as well. More specifically, the retrieval of hydrates from the shallow core of the *Malenki* crater points towards focussed near-vertical fluid migration from depth, while the plume observed in the water column just above the *Malenki* structure and the vertical chimney on the seismic data suggests gas-rich fluid expulsion from the mud volcano. The source of the clathrated biogenic gas can then either be gas that is recycled from destabilised hydrates (due to elevated heat-flow, transient flows, rapid sedimentation, etc.) or supplied via fluid migrating from deeper parts of the sedimentary basin through faults and fissures, or generated microbially in situ. At least, it proves that gas molecules can penetrate the HSZ as free gas bubbles or dissolved in pore water without being entirely clathrated at the base or within the HSZ, while part of it forms near-surface hydrates and another part escapes in the water column. Shallow gas hydrates in fluid escape structures like mud volcanoes are also reported form other areas, e.g. the Håkon Mosby Mud Volcano off Norway (Eldholm et al., 1999; Ginsburg et al., 1999; Milkov, 2000), but the intensity of heat and fluid flow is more modest in our case. In our opinion, fluid flow and resulting temperature anomalies through migration pathways (e.g. faults, fissures) represents the most plausible candidate to explain the irregular behaviour of the basal limit of hydrate occurrence or top of the free gas zone, as well as the discrepancies between inferred and measured heat-flow values observed. The latter is supported by the fact that an advective fluid flow component will modify the sub-bottom temperature profile.

Nearly all the seismic profiles in the study area show the presence of bright spots or enhanced reflections that often penetrate the BHSZ or BSR. They all represent a limited region of higher polarity-reversed reflectivity of individual lithological boundaries and hence are interpreted as local accumulation or migration of gases within the HSZ (Figs. 5a and 6a). This indicates that fluid migration within specific stratigraphic layers forms an additional migration mechanism in the axial part of the SBB, besides the more intensive fault-controlled migration. As discussed earlier, it may also be the effect of small-scale variations of in situ stability conditions, e.g. capillary forces, temperature changes in the rising fluids, changes in the chemical composition of the rising fluids or perhaps local non-equilibrium conditions. It is worth noting that, compared to the zone of common BSRs located to the SW of our study area (Vanneste et al., 2001), such enhanced reflections within the HSZ are more frequently encountered in this area with observed gas hydrate irregularities.

6.2. Conceptual model for fluid migration patterns in Lake Baikal

Advection and/or convection of heat and fluids play a dominant role in this highly dynamic geological setting. We conclude that the variations in BHSZ depths result from thermal water migration along active fault zones and venting sites, with additional migration along the dipping stratigraphy. Transient or episodic heat and fluid pulses might then also be responsible for disturbing the BHSZ, giving rise to the fluid discharge structures by hydraulic fracturing of sediments by overpressured fluids, and creating zones of elevated heat-flow or shallow BHSZ.

However, this system is far more complicated than a simple upward migration of fluids. The zone of deep BHSZ (thus low inferred heat-flow) flanking the zone of elevated heat-flow to the SSE demands another mechanism. This zone lies further away from the seepages and antithetic fault, but has more or less similar spatial dimensions. Such low heat-flow values require a downward directed recharge fluid flow, in contradiction to compaction-driven or focussed upward fluid migration that is more common in sedimentary basins. Hence, such downward fluid flow needs a driving force that goes beyond compaction-driven flow. We share the opinion that such flow pattern within the sediments can only be generated by density differences in the pore fluids, and call for a fluid convection or circulation process. A conceptual model is shown in Fig. 10. Pore fluids move upward in the zone of observed fluid discharge and the faulting, and downward S of it. Such convection cells then account for both relatively shallow BHSZ positions and deep BHSZ locations the one next to the other on relatively short distances. Fault segments, the venting sites as well as dipping strata then represent potential fluid migration pathways, for both upward and downward fluid flow. The coarse sediment layer marking the transition from slow to fast-rifting units found at about 2 km sub-bottom depths

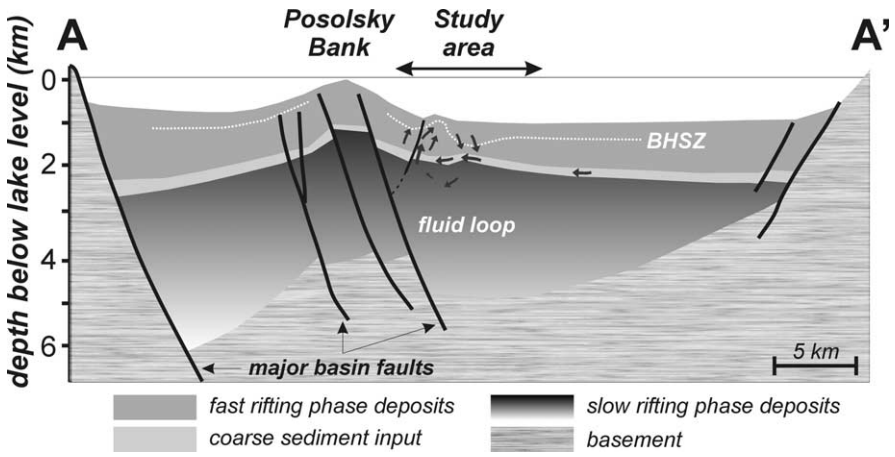

Fig. 10. Cartoon showing the concept of a fluid loop model on a cross-section of the SBB, as a hypothesis for explaining the depressions in the BHSZ. The location of this line crossing the *Malenki* mud volcano is shown in the overview Fig. 2.

may act as an important contributor for such a recharge mechanism. Furthermore, the oscillations as observed along GAHY021 (Figs. 6a and 7b,d) suggest that the inferred convection cells have laterally different intensities that may be related with the fluid discharge structures.

The driving forces for such fluid recharge can be one of the following mechanisms. (1) Gas pumping, as suggested for the Hydrate Ridge (Tryon et al., 1999), where the authors inferred a fluid loop system from surface flux data characterised by both influx and outflow in nearby stations. Similar to our observations, they report a slightly disrupted BSR. (2) Dipping bathymetry can result in lateral pore pressure density differences in a situation of nearly isothermal seafloor conditions, as discussed in Harris et al. (2000) to explain large-scale heat-flow differences in the Hawaiian apron. If so, then the Posolsky Bank and its southern boundary fault located N of the study area and rising above the SBB may be involved. (3) Salinity differences as a result of hydrate dissociation can also create pore fluid density differences, considered to play a key role in fluid convection cycles and mud volcanoes in the Barbados accretionary prism (Henry et al., 1996). It is questionable whether the salinity differences in the nearly salt-free Lake Baikal water can trigger such fluid loops. (4) The migration of gas and pore water in sediments can differ from one location to the other as a result of buoyancy, adding a net upward force component on the gas phase that will expand during upward migration. (5) An additional trigger may come from the active tectonic settings as a major zone of extension. Over the last 10 years, extensive seismicity was reported and several earthquakes with magnitudes >5 occurred, having their epicentre within the SBB (Solonenko, Solonenko, Melnikova, & Shteiman, 1997), i.e. proximal to the study area. Hence, the fluid circulation flows as we propose can be easily reinforced by such neo-tectonic activity, and subsequent heat and fluid expulsion along the intra-basinal fault systems (e.g. Posolsky fault) of Lake Baikal, disturbing and interrupting the prevailing temperature and pressure conditions. Additionally, in such a situation, the BHSZ will change its position with time and might be established in a transitional mode at non-equilibrium positions.

The fluid flow model we propose is speculative, but it provides a reasonable and feasible explanation for both the increased and depressed occurrences of the BHSZ. Additionally, fluid flow may resolve part of the ambiguity between inferred and measured heat-flow. Nevertheless, quantitative modelling of coupled conductive–advective fluid and heat transport should be performed to further work out this hypothesis and to investigate the driving forces in the SBB. This might as well shed light on the time scale involved in this complex process.

7. Conclusions

In this paper, we analysed, described, and discussed a combination of heat-flow measurements and the present-day extent of the HSZ, as inferred from SC seismic reflection profiles in the axial part of the SBB, an area characterised by faulting and mud volcanoes. Our study revealed the following:

- The BHSZ is not necessarily expressed as a BSR. Both lateral discontinuities and oscillations with significant amplitudes occur. With exception made for this non-bottom-simulating behaviour, the reflection at the BHSZ shows all characteristics typical of a common BSR (reversed polarity, relatively strong, but laterally variable amplitude, change in frequency content and amplitudes across the BHSZ, AVO effect on MC data).
- There is evidence for the migration of fluids from deeper parts of the sedimentary section towards and in some locations through the HSZ (acoustic chimney, enhanced

reflections above the BHSZ). Fluid migration takes place both through faults and fissures, and along stratigraphic boundaries.

- In nearly all cases, the measured heat-flow exceeds the inferred one. Advection may resolve part of the discrepancies between these.
- Detailed mapping of the BHSZ reflection and inversion to heat-flow reveals a zone of high heat-flow centred where the fluid escape features occur, flanked to the SSE by an area of low to modest heat-flow.
- We propose a local fluid convection mechanism driven by mainly neo-tectonic pulses in order to explain both the zones of anomalous heat-flow. This implies both lateral and temporal changes of hydrate stability that depends on the intensities of the flow pattern in the area.
- Integrated fluid flow and coupled conductive–convective heat-flow modelling should be performed to further constrain this qualitative model.

Acknowledgements

This study was supported by the Belgian OSTC (Project IN/RU/005) and the INTAS project 1915. J. Poort has a post-doctoral fellowship from the FWO-Flanders. We thank M. Grachev, O. Khlystov, A. Kremlev and A. Duchkov for logistic support, and the captains and crews of R.V. Titov and Vereshchagin for their craftsmanship. S. Guidard is acknowledged for her assistance and continuous support. W. Versteeg and W. Cresens provided onboard technical assistance. We acknowledge the reviewers and chief-editor for thoughtful comments and suggestions. We also express our gratitude to B. Lindberg for improving the text.

Appendix A

Phase boundary equation. Analytical pressure–temperature methane hydrate–fresh water–methane vapour phase equilibrium boundary, as a best fit (least squares method) using pressure P_{eq} (MPa)–temperature T_{eq} (°C) data couples taken from the program CSMHYD (Sloan, 1998), for the temperature interval of 0–25 °C

$$\log P_{eq} = a + bT_{eq} + cT_{eq}^2 \qquad \text{Vanneste (2000)}$$

$a = 0.419626$
$b = 0.039326$
$c = 0.000299$
$R^2 = 0.99.$

Sub-bottom depth z (m) vs. TWTT sub-bottom depth t (ms) based on the interval velocity profile of Golmshtok et al. (2000)

$$z = 0.0001t^2 + 0.8423t \qquad \text{Vanneste (2000)}$$

In situ pressure (MPa)

$$\textit{Hydrostatic pressure}: \; P_{hydro}\langle H,z\rangle = P_0 + 10^{-6}\rho_w g(H+z)$$

$$\text{Porosity}: \; \phi\langle z\rangle = \phi_0 \exp(-k_c z)$$

$$\phi_0 = 0.65$$

$$\text{Compaction}: \; k_c = 0.000473\ \text{m}^{-1} \qquad \text{Golmshtok et al. (2000)}$$

$$\text{Bulk density}: \; \rho\langle z\rangle = (1-\phi\langle z\rangle)\rho_m + \phi\langle z\rangle\rho_w$$

$$\rho_w = 1000\ \text{kg m}^{-3}$$

$$\rho_m = 2650\ \text{kg m}^{-3} \qquad \text{Golmshtok et al. (2000)}$$

$$\text{Lithostatic pressure}: \; P_{litho}\langle H,z\rangle$$

$$= P_{hydro}\langle H,0\rangle + 10^{-6} g \int_{z'=0}^{z'=z} \rho\langle z'\rangle \mathrm{d}z'$$

$$= P_{hydro}\langle H,0\rangle + 10^{-6} g \left\{ \rho_m z + \phi_0 \frac{\rho_m - \rho_w}{k_c} [\exp(-k_c z) - 1] \right\}$$

Geothermal gradient G (°C m^{-1})

$$G = \frac{\partial T\langle z\rangle}{\partial z} \approx \frac{T_{eq}\langle z_{BHSZ}\rangle - T_0}{z_{BHSZ}}$$

T_0 is average bottom-water temperature from CTD profiles, 3.36 °C

Thermal conductivity k (W m^{-1} K^{-1}) with depth

$$k\langle z\rangle = 1.05 + 0.001z \qquad \text{Duchkov and Kazantsev(1996)}$$

Heat-flow q (mW m^{-2})

$$q = k\langle z\rangle \frac{\partial T\langle z\rangle}{\partial z} \approx \frac{T\langle z_{BHSZ}\rangle - T_0}{\ln\left(1 + \frac{z_{BHSZ}}{1050}\right)}$$

References

Bangs, N. L., & Brown, K. M (1995). Regional heat flow in the vicinity of the Chile triple junction constrained by the depth of the bottom simulating reflection. In S. D. Lewis, J. H. Behrmann, R. J. Musgrave, & S. C. Cande (Eds.). *Proceedings of the Ocean Drilling Program, Scientific Results. Ocean Drilling Program, College Station, TX* (pp. 253–258).

Bouriak, S., Vanneste, M., & Saoutkine, A. (2000). Inferred gas hydrates and clay diapirs near the Storegga Slide on the southern edge of the Vøring Plateau, offshore Norway. *Marine Geology*, *163*, 125–148.

Clennell, M. B., Hovland, M., Booth, J., Henry, P., & Winters, P. (1999). Formation of natural gas hydrates in marine sediments. 1. Conceptual model of gas hydrate growth conditioned by host sediment properties. *Journal of Geophysical Research*, *104*(B10), 22985–23003.

Crane, K., Hecker, B., & Golubev, V. (1991). Hydrothermal vents in Lake Baikal. *Nature*, *350*, 281.

Davis, E. E., Hyndman, R. D., & Villinger, H. (1990). Rates of fluid expulsion across the Northern Cascadia Accretionary Prism: constraints

from new heat flow and multi-channel seismic reflection data. *Journal of Geophysical Research*, *95*(B6), 8869–8889.

De Batist, M., Klerkx, J., Van Rensbergen, P., Vanneste, M., Poort, J., Golmshtok, A. Y., Kremlev, A. N., Khlystov, O. M., & Krinitsky, P. (2002). Active hydrate destabilization in Lake Baikal, Siberia? *Terra Nova*, *14*(6), 436–442.

Delvaux, D., Moeys, R., Stapel, G., Petit, C., Levi, K., Miroshnichenko, A., Ruzhich, V., Sańkov, V. (1997). Paleostress reconstructions and geodynamics of the Baikal region, Central Asia. Part 2. Cenozoic rifting. *Tectonophysics*, *282*, 1–38.

Duchkov, A. D., & Kazantsev, S. A. (1996). Temperature measurements in the first underwater borehole in Lake Baikal. *Russian Geology and Geophysics*, *37*(6), 94–102.

Edgington, D. N., Klump, J. V., Robbins, J. A., Kusner, Y. S., Pampura, V. D., Sandimirov, I. V. (1991). Sedimentation rates, residence times and radionuclide inventories in lake Baikal from ^{137}Cs and ^{210}Pb in sediment cores. *Nature*, *350*, 601–604.

Eldholm, O., Sundvor, E., Vogt, P. R., Hjelstuen, B. O., Crane, K., Nilsen, A. K., Gladczenko, T. P. (1999). SW Barents Sea continental margin heat flow and Håkon Mosby Mud Volcano. *Geo-Marine Letters*, *19*, 29–37.

Ginsburg, G. D. (1998). Gas hydrate accumulation in deep water marine environments. In J.-P. Henriet, & J. Mienert (Eds.), *Gas hydrates: Relevance to world margin stability and climatic change* (pp. 51–62). Geological Society of London, Special publication.

Ginsburg, G. D., Milkov, A. V., Soloviev, V. A., Egorov, A. V., Charkashev, G. A., Vogt, P. R., Crane, K., Lorenson, T. D., Khutorskoy, M. D. (1999). Gas hydrate accumulation at the Håkon Mosby Mud Volcano. *Geo-Marine Letters*, *19*, 57–67.

Golmshtok, A. Y., Duchkov, A. D., Hutchinson, D. R., & Khanukayev, S. B. (1997). Estimation of the heat flow on Lake Baikal based on seismic data of gas hydrate lower boundary. *Russian Geology and Geophysics*, *10*.

Golmshtok, A. Y., Duchkov, A. D., Hutchinson, D. R., & Khanukaev, S. B. (2000). Heat flow and gas hydrates of the Baikal Rift Zone. *International Journal of Earth Sciences*, *89*, 193–211.

Golubev, V. A. (1982). *Geothermics of Baikal*. Novosibirsk: Nauka, 150 pp.

Golubev, V. A. (1990). Hydrothermal systems, permeability, and thermal models of the crust in the Baikal Rift Zone. *Earth Physics*, *26*, 916–924.

Golubev, V. A., Klerkx, J., & Kipfer, R. (1993). Heat flow, hydrothermal vents and static stability of discharging thermal water in Lake Baikal (south-eastern Siberia). *Bulletin des Centres de Recherches Exploration–Production Elf-Aquitaine*, *17*, 53–65.

Golubev, V. A., & Poort, J. (1995). Local heat flow anomalies along the western shore of North Baikal Basin (Zavorotny area). *Russian Geology and Geophysics*, *36*, 174–185.

Grevemeyer, I., & Villinger, H. (2001). Gas hydrate stability and the assessment of heat flow through continental margins. *Geophysics Journal International*, *145*, 647–660.

Harris, R. N., Garven, G., Georgen, J., McNukk, M. K., Christiansen, L., von Herzen, R. P. (2000). Submarine hydrogeology of the Hawaiian archipelagic apron. 2. Numerical simulations of coupled heat transport and fluid flow. *Journal of Geophysical Research*, *105*(B9), 21371–21385.

Henry, P., Le Pichon, X., Lallemant, S., Lance, S., Martin, J. B., Foucher, J.-P., Fiala-Médioni, A., Rostek, F., Guilhavmov, N., Pranal, V., Castrec, M. (1996). Fluid flow in and around a mud volcano field seaward of the Barbados accretionary wedge: results from the Manon Cruise. *Journal of Geophysical Research*, *101*, 20297–20323.

Henry, P., Thomas, M., & Clennell, M. B. (1999). Formation of natural gas hydrates in marine sediments. 2. Thermodynamical calculations of stability conditions in porous media. *Journal of Geophysical Research*, *104*(B10), 23004–23022.

von Herzen, R. P., & Uyeda, S. (1963). Heat flow through the eastern Pacific ocean floor. *Journal of Geophysical Research*, *68*, 4219–4251.

Hovland, M., & Judd, A. (1988). *Seabed pockmarks and seepages: Impact on geology, biology and the marine environment*. London: Graham & Trotman, 293 pp.

Hutchinson, D. R., Golmshtok, A. Y., Scholz, C. A., Moore, T. C., Lee, M. W., Kuzmin, M. (1991). Bottom simulating reflector in Lake Baikal. *EOS, Transactions of the American Geophysical Union*, *72*, 307.

Hutchinson, D. R., Golmshtok, A. Y., Zonenshain, L. P., Moore, T. C., Scholz, C. A., Klitgord, K. (1992). Depositional and tectonic framework of the rift basins of Lake Baikal from multi-channel seismic data. *Geology*, *20*, 589–592.

Kaul, N., Rosenberger, A., & Villinger, H. (2000). Comparison of measured and BSR-derived heat flow values, Makran accretionary prism, Pakistan. *Marine Geology*, *164*, 37–51.

Keller, G. R., Bott, M. H. P., Wendlandt, R. F., Doser, D. I., & Morgan, P. (1995). The Baikal Rift system. In K. H. Olsen (Ed.), *Continental rifts: Evolution, structure, tectonics* (pp. 325–339). *Development in Geotectonics*, Amsterdam: Elsevier.

Klerkx, J., Hus, R., De Batist, M., Van Rensbergen, P. & Poort, J (2000). The structural control of the methane venting area in the southern basin of Lake Baikal, Siberia, *VI International Conference on Gas in Marine Sediments, St Petersburg, Russia*, pp. 57.

Kuzmin, M. I., Geletoy, V. F., Kalmychkov, G., Kuznetsov, F. A., Larionov, E. G., Manakov, A. Yu., Mironov, Yu. I., Smoljakov, B. S., Dyadin, Yu. A., Duchkov, A. D., Bazin, N. M., Mahov, G. M. (2000a). The first discovery of the gas hydrates in the sediments of Lake Baikal. In G. D. Holder, & P. R. Bishnoi (Eds.), *Gas hydrates: Challenges for the future* (pp. 112–115). New York: Annals of the New York Academy of Sciences.

Kuzmin, M. I., Karabanov, E. B., Prokopenko, A. A., Gelety, V. F., Antipin, V. S., Williams, D. F., Gvozdkov, A. N. (2000b). Sedimentation processes and new age constraints on rifting stages in Lake Baikal: results from deep-water drilling. *International Journal of Earth Sciences*, *89*, 183–192.

Lachenbruch, A. H. (1968). Rapid estimation of the topographic disturbance to surfacial thermal gradients. *Review of Geophysics*, *6*, 365–400.

Lee, M. W., Hutchinson, D. R., Collett, T. S., & Dillon, W. P. (1996). Seismic velocities for hydrate-bearing sediments using weighted equation. *Journal of Geophysical Research*, *101*, 20347–20358.

Lister, C. R. B. (1970). Measurement of in situ conductivity by means of Bullard-type probe. *Geophysical Journal of the Royal Astonomical Society*, *19*, 521–533.

Logachev, N. A. (1993). History and geodynamics of the Lake Baikal Rift in the context of the Eastern Siberia Rift System: a review. *Bulletin des Centres de Recherches Exploration–Production Elf Aquitaine*, *17*, 353–370.

Logatchev, N. A., & Florensov, N. A. (1978). The Baikal system of rift valleys. *Tectonophysics*, *45*, 1–13.

Lubimova, E. A. (1969). Heat flow patterns in Baikal and other rift zones. *Tectonophysics*, *8*, 457–467.

Mats, V. D. (1993). The structure and development of the Baikal Rift depression. *Earth-Science Reviews*, *34*, 81–118.

Milkov, A. (2000). Worldwide distribution of submarine mud volcanoes and associated gas hydrates. *Marine Geology*, *167*, 29–42.

Pinneker, E. V., & Lomonosov, I. S. (1973). *On genesis of thermal waters in the Sayan–Baikal highland. Symposium on Hydrogeochemistry and Biogeochemistry*, Washington, USA: Clarke, pp. 246–253.

Poort, J (2000). *Significance of the surface heat flow in the Baikal Rift: inferences from spatial heat flow analysis and numerical modelling*. PhD Thesis. Free University of Brussels (VUB), Brussels, 112 pp.

Poort, J., & Polyansky, O. (2002). Heat transport by groundwater flow during the Baikal Rift evolution. *Tectonophysics*, *351*(1/2), 75–89.

Posewang, J., & Mienert, J. (1999). The enigma of double BSRs: indicators for changes in the hydrate stability field? *Geo-Marine Letters*, *19*, 157–163.

Ruppel, C. (1997). Anomalous cold temperatures observed at the base of the hydrate stability zone on the US Atlantic passive margin. *Geology*, *25*(8), 699–702.

Scholz, C. A., & Hutchinson, D. R. (2000). Stratigraphic and structural evolution of the Selenga Delta Accomodation Zone, Lake Baikal Rift, Siberia. *International Journal of Earth Sciences*, *89*, 212–228.

Sloan, E. D. J. (1998). *Clathrate hydrates of natural gases*. New York/ Basel: Marcel Dekker, 705 pp.

Solonenko, A., Solonenko, N., Melnikova, V., & Shteiman, E. (1997). The seismicity and earthquake focal mechanisms of the Baikal Rift Zone. *Bulletin des Centres de Recherches Exploration–Production Elf Aquitaine*, *21*, 207–231.

Sundvor, E., Eldholm, O., Gladczenko, T. P., & Planke, S. (2000). Norwegian–Greenland Sea thermal field. In A. Nøttvedt (Ed.), *Dynamics of the Norwegian Margin* (pp. 397–410). Geological Society of London, Special publication.

Tinivella, U. (1999). A method for estimating gas hydrate and free gas concentrations in marine sediments. *Bolletino di Geofisico Teoretico et Applicata*, *40*(1), 19–30.

Tryon, M. D., Brown, K. M., Torres, M. E., Tréhu, A., McManus, J., & Collier, R. W. (1999). Measurements of transience and downward fluid flow near episodic methane gas vents, Hydrate Ridge, Cascadia. *Geology*, *27*(12), 1075–1078.

Vanneste, M (2000). *Gas hydrate stability and destabilisation processes in marine and lacustrine environments: results from theoretical analyses and multi-frequency seismic investigations*. PhD Thesis. University of Gent, Gent, 255 pp.

Vanneste, M., De Batist, M., Golmshtok, A., Kremlev, A., & Versteeg, W. (2001). Multi-frequency seismic study of gas hydrate-bearing sediments in Lake Baikal, Siberia. *Marine Geology*, *172*, 1–21.

Van Rensbergen, P., De Batist, M., Klerkx, J., Poort, J., Hus, R., Vanneste, M., Granin, N., & Krinitsky, P. (2002). Sub-lacustrine mud volcanoes and cold seeps caused by dissociation of gas hydrates in Lake Baikal. *Geology*, *30*(7), 631–634.

Van Rensbergen, P., Poort, J., Kipfer, R., De Batist, M., Vanneste, M., Klerkx, J., & Granin, N. (in press). Near-surface sediment mobilization and methane venting in relation to hydrate destabilization in Southern Lake Baikal, Siberia. In P. V. Rensbergen, R. Hillis, A. Maltman, & C. Morley (Eds.), *Subsurface Sediment Mobilisation*. Geological Society of London, Special publication, 2003 in press.

Wessel, P., & Smith, W. H. F. (1991). Free software helps map and display data. *EOS Transactions of the American Geophysical Union*, *72*(41), 441 see also pp. 445–446.

Wood, W. T., & Ruppel, C (2000). Seismic and thermal investigations of the Blake Ridge gas hydrate area: a synthesis. In C. K. Paull, R. Matsumoto, P. J. Wallace, & W. P. Dillon (Eds.). *Proceedings of the Ocean Drilling Program, Scientific Results, Ocean Drilling Program, College Station, TX* (pp.253–264).

Xu, W., & Ruppel, C. (1999). Predicting the occurrence, distribution and evolution of methane gas hydrates in porous marine sediments. *Journal of Geophysical Research*, *104*, 5081–5096.

Yamano, M., Uyeda, S., Aoki, Y., & Shipley, T. H. (1982). Estimates of heat flow derived from gas hydrates. *Geology*, *10*, 339–342.

Zonenshain, L. P., Golmshtok, A. Y., & Hutchinson, D. D. (1992). The structure of the Baikal Rift. in Russian *Geotectonics*, *5*, 63–77.

Zonenshain, L. P., Kuzmin, M. I., Natapov, L. M., & Page, B. M. (1990). *Geology of the USSR: a plate-tectonic synthesis*. *AGU Geodynamics Series, 21*, American Geophysical Union, 240 pp.